Interference effects during the Auger decay of the C^*O $1s^{-1}\pi^*$ resonance studied by angular distribution of the $CO^+(A)$ photoelectrons and polarization analysis of the $CO^+(A\text{-}X)$ fluorescence

Ph. V. Demekhin,[1,*] I. D. Petrov,[2] V. L. Sukhorukov,[2] W. Kielich,[1] P. Reiss,[1] R. Hentges,[1] I. Haar,[1] H. Schmoranzer,[3] and A. Ehresmann[1]

[1]*Institute of Physics and CINSaT, University of Kassel, D-34132 Kassel, Germany*

[2]*Rostov State University of Transport Communications, 344038 Rostov-on-Don, Russia*

[3]*Department of Physics, Kaiserslautern University of Technology, D-67653 Kaiserslautern, Germany*

(Received 25 September 2009; published 23 December 2009)

Angular distributions of the $CO^+(A\ ^2\Pi)$ photoelectrons and of the $CO^+(A\ ^2\Pi \rightarrow X\ ^2\Sigma^+)$ fluorescence are computed in the vicinity of the $1s^{-1}\pi^*$ resonant excitation of the C^*O molecule. In the calculations, lifetime vibrational interference and the direct transition amplitude for population of the $A\ ^2\Pi(v')$ states were taken into account *ab initio*. The weak direct photoionization channel induces broad exciting-photon energy range dispersions of the angular distribution parameters $\beta_A^e(\omega)$ and $\beta 2_A^X(\omega)$, and the nuclear vibrational motion causes variations of the computed parameters across the positions of the $C^*O(v_r)$ vibronic states. Present calculations are in good agreement with available vibrationally and angularly resolved resonant Auger spectra. Theoretical $\beta 2_A^X(\omega)$ parameters are in agreement with the experimental results from the polarization analysis of the $CO^+(A\text{-}X)$ fluorescence induced by linearly polarized synchrotron radiation.

DOI: 10.1103/PhysRevA.80.063425 PACS number(s): 33.80.Eh, 32.80.Hd, 33.50.Dq, 33.80.−b

I. INTRODUCTION

Alignment and orientation of the residual ion in photoionization provide detailed conclusions on the emitted photoelectron partial waves [1]. The corresponding parameters are usually obtained from the angular distribution or polarization analysis of fluorescence emitted via subsequent relaxation of the ion [2–5]. Recent progress in the development of experimental and theoretical methods enabled a set of studies of the fluorescence polarization (similar to its angular distribution) in atoms (see, e.g., the review [6]). However, to our knowledge, there are neither experimental nor theoretical studies of this problem in molecules.

In the present paper we report the joint theoretical and experimental study of the angular distributions of photoelectrons and fluorescence radiation emitted in the vicinity of the C^*O $1s^{-1}\pi^*$ resonance. Here, the participator Auger decay of the core-excited state into the $CO^+(A\ ^2\Pi)$ valence-ionized state, and the subsequent $A\ ^2\Pi \rightarrow X\ ^2\Sigma^+$ fluorescence in the CO^+ ion will be studied. From our previous work on the Auger decay of Kr $3d^9np$ resonances [3–5] we know that, if the resonant photoionization channel dominates over the direct one (this applies for the C^*O excitation), the corresponding resonant features in the angular distribution parameters are much broader than in the cross sections. As demonstrated in [3–5], the weak direct photoionization channel plays an important role resulting in broad exciting-photon energy dependencies (dispersions) of the Auger electron angular distribution and residual ion polarization parameters. The influence of the weak direct photoionization channel on the decay of the C^*O resonance is, therefore, one aim of the present work.

Resonant Auger (RA) decay of the C^*O $1s^{-1}\pi^*$ core-excited molecule is one of the most thoroughly studied processes both, experimentally [7–13] and theoretically [10–16]. In the vicinity of the $1s^{-1}\pi^*$ excitation (287.4 eV) the amplitude for direct population of the final RA states is small compared to the resonant transition amplitude. Therefore, the majority of features in measured RA spectra can be satisfactorily reproduced by computations [11–14] neglecting the direct channel (i.e., applying a two-step (2ST) model for resonant excitation and Auger decay) and accounting for the lifetime vibrational interference (LVI [17]) effects in the resonant channel. First indications for the importance of the direct photoionization channel in the description of the RA spectra of the C^*O molecule were reported in [10]. In this work, the strong exciting-photon energy dependencies of the branching ratios between the integral intensities of the different participator Auger channels observed by detuning the photon energy from the resonance were explained by the presence of the weak direct channel.

The RA electron angular distribution parameters for randomly oriented CO molecules were measured with relatively low resolutions in [7,8]. The electronic parts of the anisotropy parameters were computed in [15,16] within the 2ST model, and were found in reasonable agreement with the data of [8]. The angular distribution of RA electrons was reinvestigated later with higher excitation energy and electron detection resolution [12,13], resolving vibrational structures of both initial and final Auger states. Substantial variations of measured parameters with the vibrational quantum numbers of the resonance state, v_r, and final Auger states, v', were observed in [13] and tentatively assigned to the influence of the direct photoionization channel in the presence of the LVI. Opposite results were reported in [9], where the molecule-fixed frame Auger electron angular distributions of the C^*O resonance, measured with high energy resolution and interpreted applying the 2ST model, were found to be independent of the molecular vibrational motion. Therefore, another goal of the present work is to study how the vibra-

*demekhin@physik.uni-kassel.de

tional motion in molecules influences angular distributions of the photoelectrons and fluorescence radiation.

The paper is organized as follows. The present theoretical approach is described in Sec. II. Theoretical results are discussed in Sec. III and compared with the present experiment in Sec. IV. We conclude with a brief summary.

II. THEORY

The processes relevant to the present study can be schematically represented as follows:

$$\begin{aligned}
&(G)\ \mathrm{CO}\ 2\sigma^2 1\pi^4 5\sigma^2(X\ ^1\Sigma^+, v_0=0)+\hbar\omega\\
&\downarrow \text{Resonant core excitation}\\
&(R)\ \mathrm{C^*O}\ 2\sigma^1 1\pi^4 5\sigma^2 2\pi^1(^1\Pi, v_r)\\
&\Downarrow \text{Autoionization or Direct ionization}\\
&(D)\ \mathrm{CO^+}\ 2\sigma^2 1\pi^3 5\sigma^2(A\ ^2\Pi, v')+\varepsilon\ell m\mu\\
&\downarrow \text{Fluorescence decay}\\
&(F)\ \mathrm{CO^+}\ 2\sigma^2 1\pi^4 5\sigma^1(X\ ^2\Sigma^+, v'')+\varepsilon\ell m\mu+hc/\lambda
\end{aligned} \tag{1}$$

The single and double arrows denote electric-dipole and Coulomb interaction, respectively. Linearly polarized synchrotron radiation with the energy ω around 287.4 eV excites the ground state of the CO molecule (G) into the $1s^{-1}\pi^*$, v_r vibronic resonances of the C^*O molecule (R) with their subsequent autoionization via the participator Auger decay into the $CO^+(A\ ^2\Pi, v')\varepsilon\ell m\mu$ continua (D). In addition, the direct population of the $CO^+(A\ ^2\Pi, v')$ ionic states via a $(G)\rightarrow(D)$ dipole transition takes place [not indicated in scheme (1) for brevity]. The $A\ ^2\Pi$, v' states of the CO^+ ion decay in the next step via emission of a photon in the visible fluorescence range ($\lambda=300-700$ nm [18]) into the $X\ ^2\Sigma^+$, v'' states (F).

In order to compute the transition energies and amplitudes entering scheme (1) we applied the theoretical approach developed in [19–24]. Its brief description and basic equations determining the angular distributions of photoelectrons and fluorescence radiation for diatomic molecules are discussed in the following sections.

A. General relations

We assume for simplicity that either Hund's coupling case (a) or (b) applies for the description of the diatomic molecule [25]. Thus, the initial state of the molecule can be defined as $|\alpha_0\Omega_0 v_0\rangle$, where $\Omega_0=\Lambda_0+\Sigma_0$ is the projection of the total electronic angular momentum along the molecular axis; Λ_0 and Σ_0 are the projections of the total orbital angular momentum L and the total spin S on the molecular axis; v_0 is the vibrational quantum number; and α_0 denotes the remaining quantum numbers of the initial state. The final state of the ionization process consists of a bound ionic state $|\alpha_1\Omega_1 v_1\rangle$ and a photoelectron in a continuous spectrum, which can be expanded in the asymptotical region via $|\varepsilon\ell m\mu\rangle$ partial waves [26] with fixed projections m and μ of the orbital angular momentum ℓ and spin on the molecular axis.

The angular distribution of photoelectrons after excitation by linearly and circularly polarized light for these coupling cases was derived previously in [26–28]. In the case where randomly oriented molecules are excited by linearly polarized light and the spin polarization of the photoelectrons is not resolved in the experiment, the angular distribution of the photoelectrons is described by the well known formula for the differential photoionization cross section,

$$\frac{d\sigma_{\Omega_1 v_1}(\omega)}{d\Omega}=\frac{\sigma_{\Omega_1 v_1}(\omega)}{4\pi}[1+\beta^e_{\Omega_1 v_1}(\omega)P_2(\cos\theta)], \tag{2}$$

where θ is the angle between the electric field vector of the exciting radiation and the direction of propagation of the outgoing electron emitted into the solid angle $d\Omega$. The total photoionization cross section, $\sigma_{\Omega_1 v_1}(\omega)$, entering Eq. (2) can be computed in the length form of the electric-dipole operator as

$$\begin{aligned}
\sigma_{\Omega_1 v_1}(\omega)&=\frac{4\pi^2\alpha a_0^2\omega}{3g_{\Omega_0}}\sum_{\Omega_0\Omega_1}\sum_{\ell m\mu k}|\langle\Omega_1 v_1,\varepsilon\ell m\mu|\mathbf{d}_k|\Omega_0 v_0\rangle|^2\\
&=\sum_{\Omega_0\Omega_1}\sum_{\ell m}\sum_{\mu k}|D_k(\Omega_1 v_1,\varepsilon\ell m\mu)|^2,
\end{aligned} \tag{3}$$

where $\alpha=1/137.036$ is the fine-structure constant, the square of the Bohr radius $a_0^2=28.0028$ Mb converts the atomic units for cross sections to megabarn ($1\ \mathrm{Mb}=10^{-22}\ \mathrm{m}^2$), g_{Ω_0} is the statistical weight of the initial electronic state $|\alpha_0\Omega_0\rangle$, and the energy ω is connected with the energy of the photoelectron, ε, and the energy of the $|\alpha_1\Omega_1 v_1\rangle$ state, $E_{\Omega_1 v_1}$, as: $\omega=E_{\Omega_1 v_1}+\varepsilon$. The transition amplitude $D_k(\Omega_1 v_1,\varepsilon\ell m\mu)$ defined in Eq. (3) is given in $(\mathrm{Mb})^{1/2}$. The first summation in Eq. (3) must be performed over all degenerate electronic states $|\alpha_0\Omega_0\rangle$ and $|\alpha_1\Omega_1\rangle$. In this formalism the electron angular distribution parameter, $\beta^e_{\Omega_1 v_1}(\omega)$, is given by [26]

$$\begin{aligned}
\beta^e_{\Omega_1 v_1}(\omega)=&\frac{1}{\sigma_{\Omega_1 v_1}(\omega)}\sum_{\Omega_0\Omega_1}\sum_{\ell m}\sum_{\ell' m'}\sum_{kk'}\sum_{\mu}(i)^{\ell+\ell'}\\
&\times\sqrt{30(2\ell+1)(2\ell'+1)}(-1)^{\ell'+m+k}e^{-i(\delta_{\ell m}-\delta_{\ell' m'})}\\
&\times\begin{pmatrix}\ell & \ell' & 2\\ 0 & 0 & 0\end{pmatrix}\begin{pmatrix}\ell & \ell' & 2\\ m & -m' & k'-k\end{pmatrix}\\
&\times\begin{pmatrix}1 & 1 & 2\\ -k & k' & k-k'\end{pmatrix}D_k(\Omega_1 v_1,\varepsilon\ell m\mu)\\
&\times D^*_{k'}(\Omega_1 v_1,\varepsilon\ell' m'\mu),
\end{aligned} \tag{4}$$

where $\delta_{\ell m}$ is the phase shift of the electron partial wave.

Proceeding along the same lines as suggested in [26] for treating molecular aspects of the problem we have derived equations describing the angular distribution of the fluorescence emitted in the subsequent $|\alpha_1\Omega_1 v_1\rangle\rightarrow|\alpha_2\Omega_2 v_2\rangle$ transition. The angular distribution of fluorescence for randomly oriented diatomic molecules excited by linearly polarized light is determined by the following formula for the differential fluorescence intensity:

$$\frac{dI^{\Omega_2 v_2}_{\Omega_1 v_1}(\omega)}{d\Omega} = \frac{I^{\Omega_2 v_2}_{\Omega_1 v_1}(\omega)}{4\pi}[1 + \beta 2^{\Omega_2 v_2}_{\Omega_1 v_1}(\omega) P_2(\cos\,\theta)], \quad (5)$$

where θ is the angle between the electric field vector of the exciting radiation and the direction of detection of the fluorescence radiation. In the two-step model for the photoionization and fluorescence decay, the total fluorescence intensity, $I^{\Omega_2 v_2}_{\Omega_1 v_1}(\omega)$, is a product of two terms,

$$I^{\Omega_2 v_2}_{\Omega_1 v_1}(\omega) = \sigma_{\Omega_1 v_1}(\omega) \chi^{\Omega_2 v_2}_{\Omega_1 v_1}, \quad (6)$$

where $\sigma_{\Omega_1 v_1}(\omega)$ is defined by Eq. (3), and the fluorescence yield for the $|\alpha_1 \Omega_1 v_1\rangle \rightarrow |\alpha_2 \Omega_2 v_2\rangle$ transition, $\chi^{\Omega_2 v_2}_{\Omega_1 v_1}$, is given by

$$\chi^{\Omega_2 v_2}_{\Omega_1 v_1} = \frac{\Gamma^{\Omega_2 v_2}_{\Omega_1 v_1}}{\sum_{\Omega_2 v_2} \Gamma^{\Omega_2 v_2}_{\Omega_1 v_1}}. \quad (7)$$

The total radiative width in the denominator of Eq. (7) is the sum of partial radiative widths over all accessible final vibronic states $|\alpha_2 \Omega_2 v_2\rangle$. The fluorescence probability $\Gamma^{\Omega_2 v_2}_{\Omega_1 v_1}$ (equals the partial radiative width in atomic units) is given by [29]

$$\Gamma^{\Omega_2 v_2}_{\Omega_1 v_1} = \frac{4}{3 g_{\Omega_1}} \left(\frac{2\pi}{\lambda}\right)^3 \sum_{\Omega_1 \Omega_2} \sum_q |\langle \Omega_2 v_2 | \mathbf{d}_q | \Omega_1 v_1 \rangle|^2, \quad (8)$$

where g_{Ω_1} is the statistical weight of the electronic state $|\alpha_1 \Omega_1\rangle$, and the first summation must be performed over all degenerate electronic states $|\alpha_1 \Omega_1\rangle$ and $|\alpha_2 \Omega_2\rangle$.

In the above designations the equation for the fluorescence angular distribution parameter, $\beta 2^{\Omega_2 v_2}_{\Omega_1 v_1}(\omega)$, reads:

$$\begin{aligned}\beta 2^{\Omega_2 v_2}_{\Omega_1 v_1}(\omega) = \frac{1}{B} \sum_{\Omega_0 \Omega_2} \sum_{q q'} \sum_{\Omega_1 \Omega_1'} \sum_{\ell m \mu} \sum_{k k'} 3(-1)^{k+q'+1} \\ \times \begin{pmatrix} 1 & 1 & 2 \\ k & -k' & M_k \end{pmatrix} \begin{pmatrix} 1 & 1 & 2 \\ q & -q' & -M_k \end{pmatrix} \\ \times \langle \Omega_2 v_2 | \mathbf{d}_{q'} | \Omega_1' v_1 \rangle^* \langle \Omega_2 v_2 | \mathbf{d}_q | \Omega_1 v_1 \rangle \\ \times D^*_{k'}(\Omega_1' v_1, \varepsilon \ell m \mu) D_k(\Omega_1 v_1, \varepsilon \ell m \mu), \end{aligned} \quad (9)$$

where the normalization coefficient B is equal to

$$B = \sum_{\Omega_0 \Omega_2} \sum_{\Omega_1 k q} \sum_{\ell m \mu} |\langle \Omega_2 v_2 | \mathbf{d}_q | \Omega_1 v_1 \rangle|^2 |D_k(\Omega_1 v_1, \varepsilon \ell m \mu)|^2, \quad (10)$$

and parameters k, k', q, q', and M_k must satisfy the following equality condition:

$$M_k = k' - k = q - q'. \quad (11)$$

Two remarks are necessary here. We point out that in contrast to the parameter β^e [Eq. (4)], the interference between photoionization amplitudes corresponding to different partial electron waves $|\varepsilon \ell m \mu\rangle$ is absent in Eq. (9). This fact is a consequence of the integration of the fluorescence intensity over all directions of emission of the photoelectron, since it is not observed in coincidence with the fluorescent photon. In the general case, Eq. (9) cannot be further simplified to the incoherent sum of partial photoionization cross sections (and without transition amplitudes for radiative decay) as it was possible for the atomic fluorescence angular distribution parameter [3,30]. This is due to the fact that for diatomic molecules the summations over the indices Ω_1 and Ω_1' are incomplete, since only electronic substates with $\pm|\Omega_1|$ are degenerate and substates with different absolute values $|\Omega_1|$ are nondegenerate. That is why the final equation for the parameter $\beta 2$ contains the interference between photoionization amplitudes corresponding to the population of different degenerate electronic substates $|\alpha_1 \Omega_1\rangle$ and $|\alpha_1 \Omega_1'\rangle$, and the transition amplitudes for the $|\alpha_1 \Omega_1 v_1\rangle \rightarrow |\alpha_2 \Omega_2 v_2\rangle$ radiative decay enter Eqs. (9) and (10) in an explicit form.

In order to test Eqs. (4) and (9) we applied them to the description of the following process in the He atom:

$$\begin{aligned} 2p^1 3p^1\ {}^1S_0 + \hbar\omega &\rightarrow 2p^1({}^2P_{1/2,3/2}) + \varepsilon s_{1/2}/\varepsilon d_{3/2,5/2}\ {}^1P_1 \\ &\rightarrow 1s^1\ {}^2S_{1/2} + \varepsilon s_{1/2}/\varepsilon d_{3/2,5/2} + hc/\lambda, \end{aligned}$$

which is very similar to the presently studied molecular process [Eq. (1)]. In the calculations, the He atom was first located in the coordinate origin, and the β^e and $\beta 2$ parameters were computed applying the equations valid for the atomic case [3]. The same parameters were also computed for the He atom shifted from the coordinate origin by $\Delta R = +1$ a.u. along the z axis applying Eqs. (4) and (9). In both cases we have obtained equal values for the computed angular distribution parameters.

B. Potential energy curves

The adiabatic potential energy curves were computed similarly to our recent works [19,20,22,24] using the PC GAMESS (General Atomic and Molecular Electronic Structure System) version Alex A. Granovsky (Ref. [31]) of the GAMESS (U.S.) QC package [32]. We used a triple-zeta valence (TZV) basis set [33] adding three polarization shells of d type and one of f type. A multiconfiguration self-consistent field (MCSCF) calculation choosing full valence complete active space (FVCAS) with subsequent multireference configuration interaction (MRCI) approach was applied to calculate the potential energy curves.

The results of calculations for the $X\ {}^1\Sigma^+$ ground state of the CO molecule and for the $X\ {}^2\Sigma^+$ and $A\ {}^2\Pi$ states of the CO^+ ion are depicted in Fig. 1(a). The zero of the energy scale was set to the $v=0$ vibrational level of the CO ground state and potential curves of the CO^+ were shifted by +0.3 eV [24]. The quality of the calculations was checked by computing the vibrational and rotational spectroscopic constants. The presently computed spectroscopic constants for CO and CO^+ states are found to be in good agreement with the experimental [34] ones.

In order to compute the potential energy curve of the $1s^{-1}\pi^*\ {}^1\Pi$ core-excited state of the C^*O molecule we applied the equivalent core "$Z+1$" approximation similar to our previous studies of the core-excited states of the N_2 and NO molecules [19,20]. Thus, we computed the potential curve for the $X\ {}^2\Pi$ ground state of the NO molecule. In order to

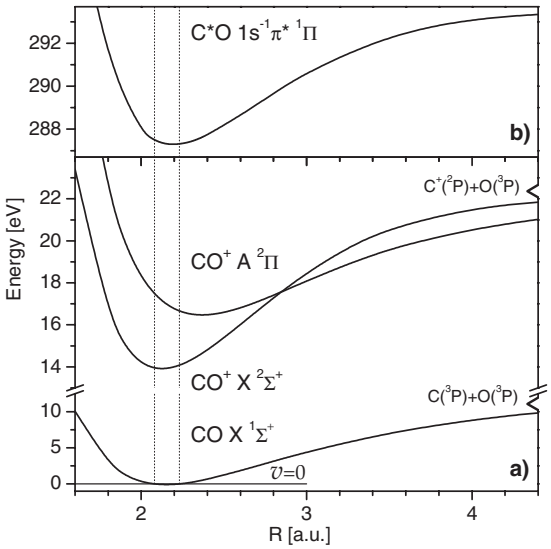

FIG. 1. Panel (a): potential energy curves computed for the $X\ ^1\Sigma^+$ ground state of CO, and the $X\ ^2\Sigma^+$ and $A\ ^2\Pi$ states of the CO^+ ion. The dissociation limits are marked by hollow triangles and the Franck-Condon region for the ground state of CO is shown by the vertical dot lines. Panel (b): potential energy curve for the $1s^{-1}\pi^*\ ^1\Pi$ core-excited state of the C*O molecule simulated in the equivalent core approximation.

eliminate a small inaccuracy of the $Z+1$ approximation we used the experimental photoionization spectrum from [11]. The total photoionization cross section calculated in the vicinity of the C*O resonance is compared with the experimental [11] one in Fig. 2. In the calculation, we utilized experimental natural widths of 80 meV [35] and the experimental energy resolution of 60 meV. The energy of the zero vibrational level, $E_{v_r=0}$, of the computed curve was set to the experimental energy of 287.40 eV [11]. Good agreement between vibrational intensity distributions in the computed and measured cross sections was obtained by applying a small shift to the equilibrium internuclear distance (Δr_e =+0.005 a.u.) of the computed potential curve. The potential curve of the $1s^{-1}\pi^*\ ^1\Pi$ state simulated as described above is depicted in Fig. 1(b) and used in the further calculations.

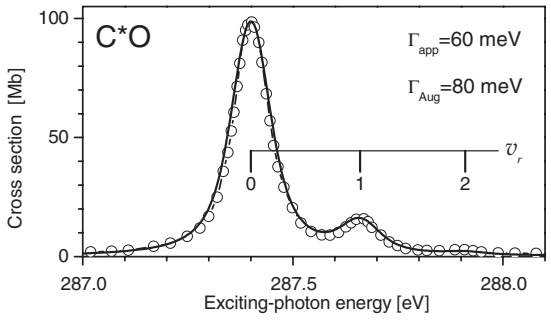

FIG. 2. Experimental C*O photoionization cross section (open circles) from [11] compared with the presently computed one (solid curve). The theoretical cross section was additionally convolved with a Gaussian of 60 meV FWHM. The maximum of the measured cross section is set to the maximum of the computed one. Positions of the v_r vibrational levels are also indicated.

C. Photoelectron molecular orbitals

In order to compute electronic transition matrix elements we applied the single center (SC) approach [36,37], which is a powerful tool to study molecular photoabsorption [20,22–24]. According to the SC method the molecular orbital (MO) of a diatomic molecule (where the projection m of the angular momentum ℓ along the internuclear axis is conserved) is represented as an expansion by spherical harmonics, $Y_{\ell m}(\theta,\varphi)$, with respect to the center (midpoint between the two nuclei),

$$\Psi_{nm}(x,y,z)=\sum_{\ell}\frac{P_{n\ell m}(r)}{r}Y_{\ell m}(\theta,\varphi), \tag{12}$$

where r, θ, φ are the coordinates with respect to the center, $P_{n\ell m}(r)$ stands for the radial parts of the partial harmonics in the SC expansion of the MO.

The radial parts $P_{n\ell m}(r)$ of the photoelectron molecular orbital satisfy the following system of coupled differential Hartree-Fock equations [23,24,37],

$$\sum_{\ell'}\left\{\left[-\frac{d^2}{dr^2}+\frac{\ell(\ell+1)}{r^2}-\varepsilon_{nm}\right]\delta_{\ell\ell'}+V^{ne}_{\ell\ell'}(r)+V^{ee}_{\ell\ell'}(r)\right\}P_{n\ell' m}(r)=0, \tag{13}$$

under the following normalization conditions for the discrete and continuous spectra:

$$\sum_{\ell}\langle P_{n\ell m}|P_{n'\ell m'}\rangle=\delta_{nn'}\delta_{mm'},$$

$$\sum_{\ell}\langle P_{\varepsilon\ell m}|P_{\varepsilon'\ell m'}\rangle=\delta(\varepsilon-\varepsilon')\delta_{mm'}. \tag{14}$$

In the system of Eqs. (13) the following designations are used: ε_{nm} is the one-electron energy measured in Rydberg units, $V^{ne}_{\ell\ell'}(r)$ is the potential describing nuclear-electron interaction, and $V^{ee}_{\ell\ell'}(r)$ is the potential describing direct and exchange electrostatic Coulomb interactions of the photoelectron with the ionic core. Due to a nonspherical molecular field, the system of Eqs. (13) contains the off-diagonal potentials with $\ell\neq\ell'$, which couples the equations for the different partial waves. These potentials were calculated using the LCAO MOs of the occupied shells deconvolved as Eq. (12).

The method for numerically solving the system of integrodifferential Eqs. (13) is described in detail in [23]. Therefore, only its essentials relevant for the solution in the continuous spectrum, $\varepsilon_{nm}>0$, are outlined below. In the case of interaction of M continuous spectra at a fixed energy, one obtains M degenerate M-component solutions. According to [38], linearly independent solutions of the system of Eqs. (13) at $r\to\infty$ should be sought in the following asymptotic form:

$$P^L_\ell(r)=\delta^L_\ell J_\ell(r)+\mathbb{R}^L_\ell H_\ell(r),\quad \forall\ L,\ell=1\ldots M. \tag{15}$$

Here $J_\ell(r)$ and $H_\ell(r)$ are so-called Coulomb functions (the linearly independent and normalized on the energy scale solutions in the spherically symmetric Coulomb potential). The superscript L in expression (15) numerates the different degenerate multicomponent solutions, and the subscript ℓ numbers the different components of each solution. The $M\times M$ matrix $\mathbb{R}_\ell^L$ in expression (15) is referred to as the reaction matrix or R matrix, and δ_ℓ^L is the Kronecker symbol.

The new solutions, $\mathcal{P}_\ell^L(r)$, which are normalized on the energy scale according to Eq. (14), satisfy the condition of mutual orthogonality, and describe the observable incoming-wave channels (outgoing spherical waves only in channel $\ell=L$), should be chosen as the following linear combinations of the solutions (15) [39],

$$\mathcal{P}_\ell^L = \sum_{L'}\left\{\sum_{L''}\tilde{\mathbb{U}}_{L'}^{L''}\cos\ \eta_{L''}e^{-i\eta_{L''}}\mathbb{U}_{L''}^{L}\right\}P_\ell^{L'}, \tag{16}$$

where $\mathbb{U}_{L'}^L$ and η_L are the solutions of the eigenvalue problem for the R matrix,

$$\sum_{L'}\mathbb{R}_\ell^{L'}\mathbb{U}_{L'}^L = -\tan\ \eta_L\mathbb{U}_\ell^L. \tag{17}$$

The inhomogeneous (due to exchange Coulomb interaction) system of coupled Eq. (13) can be solved, for instance, iteratively [23]. In the present work, the system (13) and integral equations for exchange Coulomb potentials were reduced to a united homogeneous system of coupled differential equations relative to both, partial harmonics and corresponding exchange potentials, as suggested in [40] and described in details in [38]. Solution of the system (13) becomes essentially easier if one takes into account the persistency of the shape of $P_{n\ell m}$ functions at high ℓ values. That allows the restriction of the expansion (12) for CO to $\ell\leq 20$, increasing the $V_{\ell\ell'}^{ne}(r)$ and $V_{\ell\ell'}^{ee}(r)$ potentials for large ℓ [24].

D. Transition amplitudes

The partial transition amplitude for the population of the $|\alpha_1\Omega_1 v_1\rangle$ vibronic state from the initial $|\alpha_0\Omega_0 v_0\rangle$ state of a molecule in the vicinity of the $|\alpha_r\Omega_r v_r\rangle$ resonances is given by (cf. also [3,41])

$$D_k(\Omega_1 v_1,\varepsilon\ell m\mu) = \sqrt{\frac{4\pi^2\alpha a_0^2\omega}{3g_{\Omega_0}}}\left\{\langle\Omega_1 v_1,\varepsilon\ell m\mu|\mathbf{d}_k|\Omega_0 v_0\rangle + \sum_{\Omega_r v_r}\frac{\langle\Omega_1 v_1,\varepsilon\ell m\mu|\dfrac{1}{|\mathbf{r}_{12}|}|\Omega_r v_r\rangle\langle\Omega_r v_r|\mathbf{d}_k|\Omega_0 v_0\rangle}{\omega-E_{\Omega_r v_r}+\dfrac{i}{2}\Gamma_{\Omega_r}}\right\}, \tag{18}$$

where $E_{\Omega_r v_r}$ are the energies of the vibronic resonances $|\alpha_r\Omega_r v_r\rangle$, and their natural widths, Γ_{Ω_r}, are assumed to be independent of the quantum number v_r. The amplitude for direct photoionization (the first term) and different resonant amplitudes (the sum over the indices $\Omega_r v_r$), enter the total transition amplitude (18) coherently.

Spin-orbit interaction of the 1π electrons results in the nondegeneracy of the $\Omega_1=\pm\frac{1}{2}$ and $\Omega_1=\pm\frac{3}{2}$ fine-structure components of the CO^+ $A\ ^2\Pi(\Omega_1)$ state. This nondegeneracy is the reason for the appearance of two components of each vibrational band of the $CO^+(A\ ^2\Pi\rightarrow X\ ^2\Sigma^+)$ fluorescence spectrum corresponding to the $\Omega_1=\pm\frac{1}{2}\rightarrow\Omega_2=\pm\frac{1}{2}$ and $\Omega_1=\pm\frac{3}{2}\rightarrow\Omega_2=\pm\frac{1}{2}$ transitions (typical separation is about $\Delta\lambda=3$ nm at $\lambda=500$ nm [18]). Therefore, it is important to consider these states as nondegenerate ones, especially in the description of the fluorescence angular distribution. In the calculations of radial integrals we neglect, however, the spin-orbit interaction of the 1π electrons. In addition, we neglect the spin-orbit interaction in the continuous spectrum. These approximations result in equal values of the spectroscopic characteristics computed separately for the degenerate $A\ ^2\Pi(\Omega_1=\pm\frac{1}{2})$ states and for the degenerate $A\ ^2\Pi(\Omega_1=\pm\frac{3}{2})$ states,

$$\sigma_{A1/2}(\omega)=\sigma_{A3/2}(\omega),\quad \beta_{A1/2}^e(\omega)=\beta_{A3/2}^e(\omega), \tag{19a}$$

$$I_{A1/2}^{X1/2}(\omega)=I_{A3/2}^{X1/2}(\omega),\quad \beta 2_{A1/2}^{X1/2}(\omega)=\beta 2_{A3/2}^{X1/2}(\omega). \tag{19b}$$

The transition amplitudes (18) were computed in the present work within the Franck-Condon approximation. The electronic matrix elements were computed at the equilibrium internuclear distance of the ground state of CO, $r_e=2.13$ a.u. [34]. In the calculations of the transition amplitudes [Eq. (18)] the relaxation of the molecular core was taken into account similar to our previous study of RA decay in atoms [3]. Calculations were performed within the sudden approximation [42] applying the theory of nonorthogonal orbitals [43].

The presently computed oscillator strength for the $2\sigma\rightarrow 2\pi$ excitation into the C^*O resonance is equal to $f_{2\sigma}^{2\pi}=0.158$ a.u. (in dimensional units $\sigma_{2\sigma}^{2\pi}=0.637$ Mb a.u.). It is in good agreement with the oscillator strength of $f_{2\sigma}^{2\pi}=(0.167\pm 0.02)$ a.u. measured in [44]. The total cross section for the direct population of the $CO^+A\ ^2\Pi$ state computed at the position of the resonance is equal to $\sigma_A^{dir}(287.4\text{ eV})=0.0350$ Mb. It is the sum of the partial cross sections corresponding to the production of the $\varepsilon\sigma$, $\varepsilon\pi$, and $\varepsilon\delta$ photoelectrons, which are equal to $\sigma_{A\varepsilon\sigma}^{dir}(287.4\text{ eV})=0.0060$ Mb, $\sigma_{A\varepsilon\pi}^{dir}(287.4\text{ eV})=0.0105$ Mb, and $\sigma_{A\varepsilon\delta}^{dir}(287.4\text{ eV})=0.0185$ Mb, respectively. The total theoretical cross section σ_A^{dir} agrees very well with the experimental data from [8] measured off-side (left and right) the resonance: $\sigma_A^{expt}(284\text{ eV})=0.036\ 37$ Mb and $\sigma_A^{expt}(292\text{ eV})=0.032\ 26$ Mb. The partial width computed for the participator Auger decay of the C^*O resonance into the $CO^+A\ ^2\Pi$ channel is equal to $\Gamma_{\pi^*}^A=4.53$ meV. It is the sum of partial widths corresponding to the production of the $\varepsilon\sigma$ and $\varepsilon\delta$ photoelectrons, which are equal to $\Gamma_{\pi^*}^{A\varepsilon\sigma}=1.07$ meV and $\Gamma_{\pi^*}^{A\varepsilon\delta}=3.46$ meV, respectively. For a comparison with experiment see discussion at the end of Sec. III A 1.

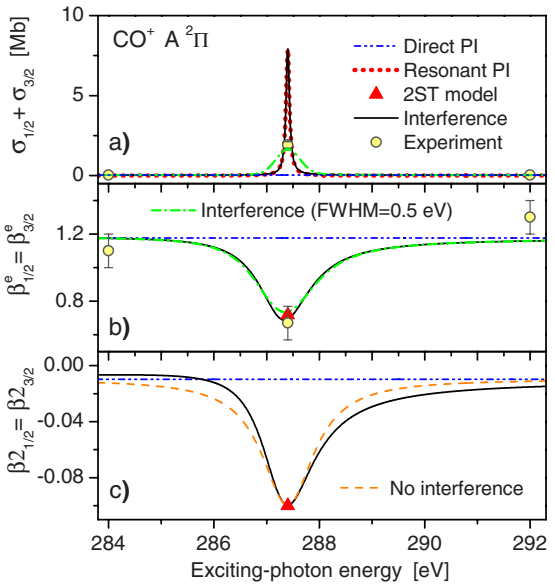

FIG. 3. (Color online) Results of the model calculations performed without accounting for molecular vibrational motion. Panel (a): cross section for the population of the $CO^+A\ ^2\Pi$ electronic state in the vicinity of the C^*O resonance. Panel (b): angular distribution parameter for the $CO^+A\ ^2\Pi$ photoelectrons. Panel (c): angular distribution parameter for the $CO^+(A\ ^2\Pi \rightarrow X\ ^2\Sigma^+)$ fluorescence. Computed parameters additionally convolved with a Gaussian of 0.5 eV FWHM are shown in panels (a) and (b) by dash-dotted curves. Open circles: experiment [8].

III. RESULTS AND DISCUSSION

In what follows we analyze angular distribution parameters for the $CO^+(A\ ^2\Pi)$ photoelectrons and for the subsequent $CO^+(A\ ^2\Pi \rightarrow X\ ^2\Sigma^+)$ fluorescence computed in the vicinity of the C^*O resonance. Electronic parts of the transition amplitude [Eq. (18)] are discussed in Sec. III A, whereas the influence of the nuclear vibrational motion is analyzed in Sec. III B.

A. Electronic transition amplitudes

In this subsection we investigate the influence of the direct electronic transition amplitude on the computed spectral characteristics. For this purpose the model calculations neglecting the molecular vibrational motion were performed. The results of the model calculations are depicted in Fig. 3. Calculations were performed within several approximations:

(i) *Direct PI*: the direct transition amplitude only was accounted for;

(ii) *Resonant PI or 2ST model*: the resonant photoionization amplitude only was accounted for;

(ii) *Interference*: interference between the direct and resonant amplitudes was taken into account;

(iv) *No interference*: the direct and resonant amplitudes were taken into account incoherently.

1. Cross section and photoelectron angular distribution

One can see from Fig. 3 that the resonant photoionization channel almost entirely determines the absolute photoionization cross section in the vicinity of the C^*O resonance [$\sigma_A^{dir}(287.4\ \text{eV}) = 0.035\ \text{Mb} \ll \sigma_A^{res}(287.4\ \text{eV}) = 7.88\ \text{Mb}$]. If one neglects the direct transition amplitude, the 2ST model applies for the interpretation of the RA decay. As a result the angular distribution parameter is independent of the exciting-photon energy and equals in our case $\beta_A^e(287.4\ \text{eV}) = 0.72$. The parameter $\beta_A^e(\omega)$ computed within the direct PI approximation is practically constant in the vicinity of the resonance, since the direct amplitude varies only slightly in this energy interval. Its presently computed value is equal to 1.18.

Being included in the calculations, the direct transition amplitude influences the computed photoionization cross section negligibly (solid and thick dotted curves in panel (a) are practically indistinguishable). On the other hand, the direct amplitude gives rise to the exciting-photon energy dependence of the computed angular distribution parameter [solid curve in the panel (b)]. One can see that the resonant channel significantly influences the computed $\beta_A^e(\omega)$ far away from the resonance, and the corresponding resonant profile in the $\beta_A^e(\omega)$ is much broader than in the $\sigma_A(\omega)$. It is straightforward to show analytically that, if the direct amplitude is much weaker than the resonant one (Fano's parameter $|q| \gg 1$), the ratio between the full widths at half-maximum (FWHMs) of resonant profiles in the angular distribution parameter and in the cross section is approximately equal to $\sqrt{\sigma_A^{res}/\sigma_A^{dir}}$, which in the present case yields a ratio of 15.

The experimental values of the $\sigma_A(\omega)$ and $\beta_A^e(\omega)$ measured in [8] at three energies around the resonance are depicted in Fig. 3 by open circles with error bars. The exciting-photon energy resolution in the experiment [8] was about 0.5 eV. Resolution of the electron detection was not enough to resolve vibrational structure of the $CO^+A\ ^2\Pi(v')$ state. Therefore, we compare the model $\sigma_A(\omega)$ and $\beta_A^e(\omega)$ with these experimental data. The theoretical parameters additionally convolved with a Gaussian of 0.5 eV FWHM are shown in the uppermost and middle panels of Fig. 3 by dash-dotted curves. Good agreement between the computed and measured $\sigma_A(\omega)$ and $\beta_A^e(\omega)$ is obvious from Fig. 3. The value of the computed photoionization cross section at its maximum of 1.65 Mb agrees with the measured value of $\sigma_A^{expt}(287.4\ \text{eV}) = 1.918 \pm 0.2$ Mb [8]. The latter fact confirms that the presently computed partial width, $\Gamma_{\pi^*}^A = 4.53$ meV, provides a correct rate for the participator Auger decay of the C^*O resonance into the $CO^+A\ ^2\Pi$ channel: $\chi_{\pi^*}^A = \Gamma_{\pi^*}^A/\Gamma_{\pi^*} = 4.53/80 = 5.66\%$.

2. Fluorescence angular distribution

In the presently considered case one can proceed with simplifications of Eq. (9) for the fluorescence angular distribution parameter. For this purpose we notice that the crossed terms with $\Omega_1' \neq \Omega_1$ in Eq. (9), corresponding to the amplitudes for population of different degenerate electronic substates $|\alpha_1\Omega_1\rangle$ and $|\alpha_1\Omega_1'\rangle$, are absent owing to the required condition (11). This is due to the fact that for the $|\Omega_1 = \frac{1}{2}\rangle$ state summations in Eq. (9) must be performed over the two degenerate substates with Ω_1, $\Omega_1' = \pm\frac{1}{2}$, and for the $|\Omega_1 = \frac{3}{2}\rangle$ state—with Ω_1, $\Omega_1' = \pm\frac{3}{2}$, separately. If one would neglect

the fine-structure splitting of the $CO^+A\ ^2\Pi$ state and assume these states as degenerate, the corresponding crossed terms with $\Omega_1' \neq \Omega_1$ were allowed in Eq. (9) for the $\varepsilon\sigma$-photoelectrons. The absence of the $\Omega_1' \neq \Omega_1$ terms for the nondegenerate states is due to the interaction of the total orbital momentum L and total spin S of the ion via the spin-orbit operator. This effect is the analog of disalignment processes of polarized ionic states of atoms [45].

In addition, the values of the radiative decay probabilities $|\langle\Omega_2 v_2|\mathbf{d}_q|\Omega_1 v_1\rangle|^2$ entering Eq. (9) are independent of the signs of the $\pm\Omega_1$ and $\pm\Omega_2$. As a result, in our case, Eq. (9) can be rewritten as the incoherent sum of partial photoionization cross sections, similarly to the atomic fluorescence angular distribution parameter [3,30],

$$\beta 2^{X\Omega_2}_{A\Omega_1^2}(\omega) = \frac{-\frac{1}{10}\sigma_{A\Omega_1\varepsilon\sigma}(\omega) + \frac{1}{5}\sigma_{A\Omega_1\varepsilon\pi}(\omega) - \frac{1}{10}\sigma_{A\Omega_1\varepsilon\delta}(\omega)}{\sigma_{A\Omega_1}(\omega)}, \tag{20}$$

where the kinematics coefficients are the same for the $|\Omega_1 = \frac{1}{2}\rangle$ and $|\Omega_1 = \frac{3}{2}\rangle$ initial fluorescence states. One can see that the value of the parameter $\beta 2$ is independent of the transition amplitudes for radiative decay into the $X\ ^2\Sigma^+(v'')$ states, which cancel in Eq. (20) due to the normalization coefficient [Eq. (10)]. More importantly, it is independent of the vibrational quantum number v''. As a consequence, one should expect similar angular distributions for all fluorescence bands within the $A\ ^2\Pi(v'=\text{const}) \rightarrow X\ ^2\Sigma^+(v'')$ vibrational progression.

If the exciting-photon energy is tuned off the resonance, one can neglect the resonant photoionization channel. Applying the values of the partial direct cross sections listed in Sec. II D, Eq. (20) yields the value of $\beta 2^X_A(\omega) = -0.01$ (direct PI). Due to the symmetry of the final state "ion+electron" the resonant photoionization is possible only into the $\varepsilon\sigma$ and $\varepsilon\delta$ channels. Therefore, on the top of the resonance one can neglect the partial photoionization cross section into the $\varepsilon\pi$ channel: $\sigma^{res}_{Av'\varepsilon\sigma}, \sigma^{res}_{Av'\varepsilon\delta} \gg \sigma^{dir}_{Av'\varepsilon\pi}$. As a result, Eq. (20) yields the value of $\beta 2^X_A(287.4\ \text{eV}) = -0.1$ (2ST model). Accounting for the direct transition amplitude results in the dispersion of the $\beta 2^X_A(\omega)$ parameter (interference). The dispersion has a wide energy range and covers about 15 natural widths around the resonance.

We note that the dispersions of the parameters $\beta^e_A(\omega)$ and $\beta 2^X_A(\omega)$ across the resonance appear even though the direct transition amplitude is included in the calculations incoherently with the resonant one. This fact is demonstrated only for the fluorescence angular distribution parameter in the lowest panel of Fig. 3, where the $\beta 2^X_A(\omega)$ computed in the no interference approximation is depicted. By comparing the solid and dashed curves, one can see that the interference influences the shape of the resonant profile in the $\beta 2^X_A(\omega)$ parameter (but not its width) making it asymmetric.

B. Nuclear vibrational motion

The accuracy of the present calculations was tested by computing the RA spectra of the C^*O molecule. The presently computed integral intensities of the participator $1s^{-1}\pi^* \rightarrow A\ ^2\Pi$ Auger spectra (solid circles) are compared in Fig. 4 with the integral intensities computed (solid triangles) and measured (open squares) in [13]. One can see from this figure that the present calculations reproduce the resonant structures of the vibrationally resolved participator RA spectra measured in [13] better than calculations from [13].

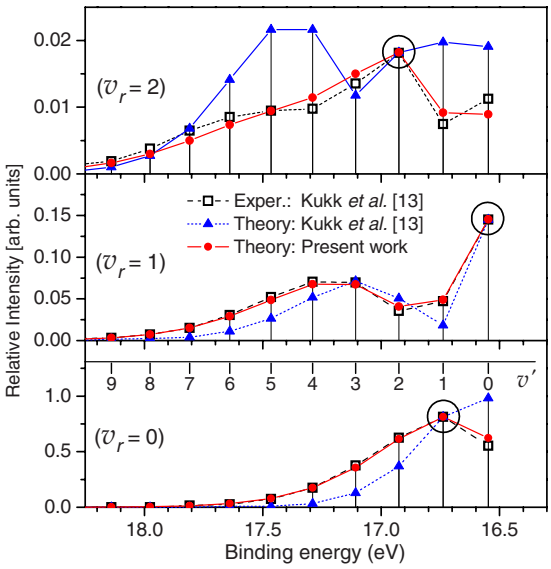

FIG. 4. (Color online) Computed and measured [13] integral intensities of the $CO^+A\ ^2\Pi(v')$ participator RA spectra. Excitation energies correspond to the positions of the $v_r=0$ (lowest panel), $v_r=1$ (middle panel), and $v_r=2$ (uppermost panel) vibrational levels of the intermediate C^*O resonance. Intensities emphasized by open circles are equalized in the measured and computed RA spectra. Positions of the v' vibrational levels are indicated by vertical bars.

Results of the present calculations of the photoionization cross sections and angular distribution parameters for photoelectrons and for fluorescence radiation (experiment description see below) are summarized in Figs. 5–8 for the $CO^+A\ ^2\Pi(v'=0-3)$ states, respectively. Calculations were performed within several approximations:

(i) *With LVI*: the direct photoionization channel and the LVI were accounted for in the calculations;

(ii) *Without LVI*: the LVI was excluded from the calculations;

(iii) *2ST model*: the direct photoionization channel was excluded from the calculations;

(iv) *No vibrations*: calculations without accounting for the nuclear vibrational motion.

By comparing the solid and dashed curves in the panels (b) and (c) of Figs. 5–8, one can see that vibrational structures of the electronic states involved in the RA decay result in substantial variations of the computed angular distribution parameters. These variations are distinct even for the weakly populated intermediate vibrational states $v_r=2-4$, which are practically invisible in the cross sections. The shape of the above variations in the computed angular distribution parameters is determined not only by the absolute value (like intensities of RA spectra), but also by the sign of the product of the two Franck-Condon factors corresponding to the excitation and subsequent Auger decay of the resonance,

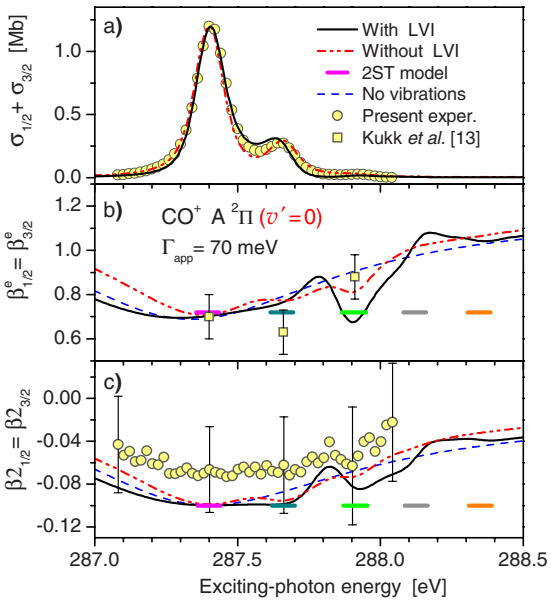

FIG. 5. (Color online) Comparison between the theory and experiment. Panel (a): Cross section for the population of the $CO^+A\ ^2\Pi(v'=0)$ vibronic state in the vicinity of the C^*O resonance. Panel (b): angular distribution parameter for the $CO^+A\ ^2\Pi(v'=0)$ photoelectrons. Panel (c): angular distribution parameter for the $A\ ^2\Pi(v'=0)\rightarrow X\ ^2\Sigma^+(v'')$ fluorescence bands progression. The computed parameters were additionally convolved with a Gaussian of 70 meV FWHM corresponding to the present experimental resolution.

$\langle v'|v_r\rangle\langle v_r|v_0\rangle$, providing an additional tool for studying nuclear dynamics accompanying the RA decay.

Panels (a) of Figs. 5–8 illustrate a small but visible influence of the LVI on the computed $\sigma_{Av'}(\omega)$. This fact is in accordance with conclusions from [11,13]. The angular distribution parameters are more sensitive to the interference

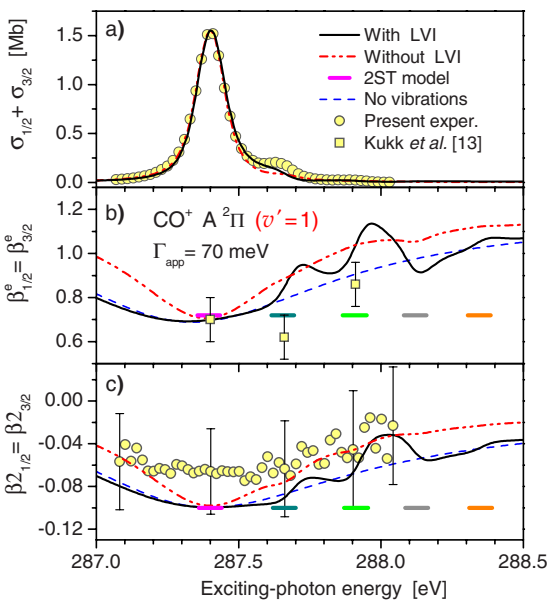

FIG. 6. (Color online) Parameters computed and measured for the $CO^+A\ ^2\Pi$ ($v'=1$) state (see notations in Fig. 5).

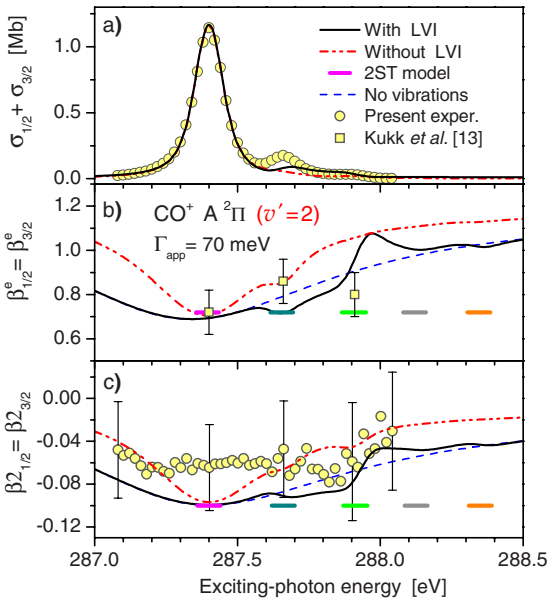

FIG. 7. (Color online) Parameters computed and measured for the $CO^+A\ ^2\Pi$ ($v'=2$) state (see notations in Fig. 5).

effects than the total cross sections [3–5], being the result of the interplay between partial photoionization amplitudes. From panels (b) and (c) one can conclude that in the presence of the direct photoionization channel the LVI influences the computed dispersions $\beta^e_{Av'}(\omega)$ and $\beta2^{Xv''}_{Av'}(\omega)$ considerably, although the energy separation between the v_r levels of the C^*O resonance, ω_e=250 meV [11], is about three times larger than their natural lifetime width, Γ_{π^*}=80 meV [35].

If one neglects the weak direct photoionization channel the computed angular distribution parameters become independent of the exciting-photon energy (of the v_r) even though the nuclear vibrational motion and LVI are included.

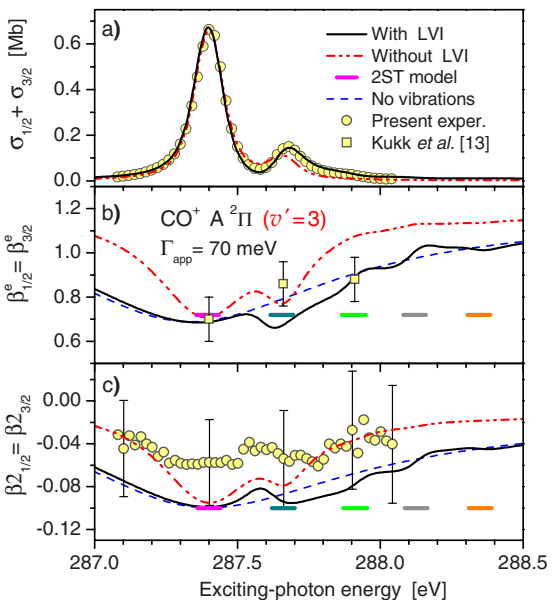

FIG. 8. (Color online) Parameters computed and measured for the $CO^+A\ ^2\Pi$ ($v'=3$) state (see notations in Fig. 5).

Indeed, within the Franck-Condon approximation and in absence of the direct photoionization channel, the complete vibrational part of the transition amplitude [Eq. (18)] cancels in the numerators and denominators of Eqs. (4) and (9). As a result, the computed values of the angular distribution parameters are determined only by the electronic part of the resonant transition amplitude, which is the same for all intermediate and final vibrational states. These values of $\beta^{e}_{Av'}=0.72$ and $\beta^{X_{v''}}_{Av'}=-0.1$ are depicted in Figs. 5–8 for all final vibronic states $A\ ^2\Pi(v')$ and each v_r level by horizontal bars with lengths equal to $\Gamma_{\pi^*}=80$ meV (2ST model).

Computed parameters $\beta^{e}_{Av'}(\omega)$ are compared in the panels (b) of Figs. 5–8 with vibrationally resolved angular distribution parameters for RA electrons measured in [13] for different $A\ ^2\Pi(v')$ vibronic states at the positions of the $v_r=0$, 1, and 2 resonances (open squares). One can see that interference effects accounted for in the present calculations qualitatively explain variations of the $\beta^{e}_{Av'}$ values on both vibrational quantum numbers, v_r and v', observed in [13]. Small disagreement between computed and measured $\beta^{e}_{Av'}$ values may be due to the presently applied Franck-Condon approximation.

IV. EXPERIMENT

The photon-induced fluorescence spectroscopy (PIFS) [46] has already been applied for polarization analysis of atomic fluorescence [3,30,47] and for studying core-excited molecules [19–21]. The present experimental setup is quite similar to these experiments.

The experiments were performed at the U49/2 PGM1 beamline, BESSY II, Berlin. A 600 lines/mm grating was used to monochromatize the linearly polarized synchrotron radiation which was then focused into a differentially pumped target cell filled with carbon monoxide at room temperature and at a pressure of 26.7 μbar. The exciting-photon energy was varied from 287.08 to 288.02 eV in steps of 20 meV. A bandwidth of the exciting radiation of about 70 meV FWHM at 287.4 eV was achieved in order to be in the resonant Raman regime for core excitations, since the natural widths of the C*O resonance is equal to 80 meV [35]. The exciting-photon energy was calibrated to the known [11] energy positions of the $1s^{-1}\pi^*$, v_r vibrational levels.

Fluorescence radiation between 378 and 578 nm was observed perpendicular to the exciting-photon beam and perpendicular to the $\vec{E}$ vector of the linearly polarized exciting radiation. The fluorescence was dispersed by a 1-m-normal-incidence monochromator equipped with a 600 lines/mm grating and recorded with a two-dimensional position-sensitive detector based on resistance anode. The resolution of this "monochromator-detector" combination was about $\Delta\lambda_{fl}=0.5$ nm. The polarization of the fluorescence radiation in the visible spectral range was analyzed by a Wollaston prism in front of the detector [47]. The prism splits the fluorescence radiation into two components ($I_\parallel$ and $I_\perp$) polarized parallel or perpendicular to the electric field vector of the synchrotron radiation, respectively. The angular separation of the two beams leaving the Wollaston prism symmetrically with respect to the optical axis amounts to 5°. Due to this separation two spectra appear simultaneously in the focus plane of the monochromator, i.e., on the position-sensitive detector. At each energy those two spectra were analyzed, yielding $I_\parallel(\omega,\lambda)$ and $I_\perp(\omega,\lambda)$.

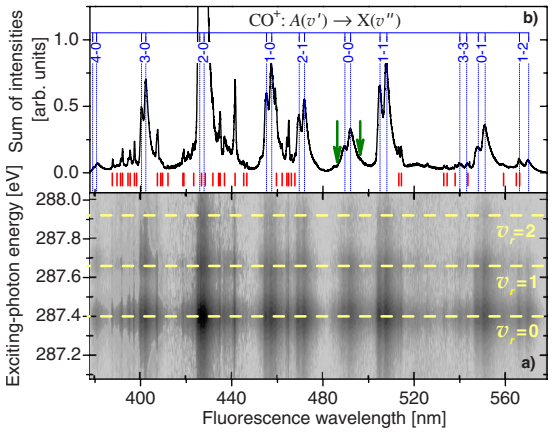

FIG. 9. (Color online) The fluorescence spectrum measured for the $I_\parallel(\omega,\lambda)$ component in the vicinity of the C*O resonance (287.08–288.02 eV) and in the wavelength range from 378 to 578 nm. (a) Dispersed fluorescence yield as a function of the exciting-photon energy in a logarithmic grayscale. Energy positions of the v_r vibrational levels from [11] are indicated by horizontal dashed lines. (b) Fluorescence intensities integrated over the present exciting-photon energy range. Positions of the $CO^+(A\text{-}X)$ doublet vibrational bands from [18] are shown by vertical dotted lines. Positions of lines corresponding to transitions in CI, CII, OI, and OII fragments according to [48] are indicated at the bottom by vertical bars.

Experimental results

The two-dimensional fluorescence spectrum measured for the $I_\parallel(\omega,\lambda)$ component is displayed in Fig. 9. Figure 9(a) shows the counts recorded by the fluorescence detector, normalized for the exciting-photon flux. Assignments of the observed $A\ ^1\Pi(v')\rightarrow X\ ^1\Sigma^+(v'')$ vibrational bands according to [18] are shown at the top of the Fig. 9(b) by vertical dotted lines, where the intensities integrated over the present exciting-photon energies are also shown. In the present fluorescence range, the $0\rightarrow1$ and $0\rightarrow0$, $1\rightarrow1$, $2\rightarrow1$, and $3\rightarrow0$ bands of the $A\rightarrow X$ system are well resolved. The other fluorescence bands were either blended by transitions in atomic fragments [marked at the bottom of Fig. 9(b)], or too weak to be resolved.

In order to analyze energy dependencies of the fluorescence intensities we introduced the integrated fluorescence intensities similar to our previous papers [19,20]. Relative integrated fluorescence intensities for the $A\ ^1\Pi(v')\rightarrow X\ ^1\Sigma^+(v'')$ bands at a given exciting-photon energy, $I_\parallel(\omega)$ and $I_\perp(\omega)$, have been determined by integrating the measured fluorescence intensities, $I_\parallel(\omega,\lambda)$ and $I_\perp(\omega,\lambda)$, over the wavelength intervals centered around the vibrational band positions as illustrated in Fig. 9(b) for the $0\rightarrow0$ band by vertical arrows,

$$I_{\parallel/\perp}(\omega) = \int I_{\parallel/\perp}(\omega,\lambda)d\lambda. \tag{21}$$

Equation (22) reveals relations between the $I_{\parallel}(\omega)$ and $I_{\perp}(\omega)$, the angular distribution parameter $\beta 2(\omega)$ and the total fluorescence intensity $I(\omega)$ for the present experimental geometry according to [2],

$$I(\omega) = \frac{2}{3}[2I_{\perp}(\omega) + I_{\parallel}(\omega)], \tag{22a}$$

$$\beta 2(\omega) = \frac{I_{\perp}(\omega) - I_{\parallel}(\omega)}{2I_{\perp}(\omega) + I_{\parallel}(\omega)}. \tag{22b}$$

Results of the present measurements are shown by open circles in panels (a) and (c) of Fig. 5 (for the $0 \rightarrow 1$ and $0 \rightarrow 0$ bands), Fig. 6 (for the $1 \rightarrow 1$ band), Fig. 7 (for the $2 \rightarrow 1$ band), and Fig. 8 (for the $3 \rightarrow 0$ band).

One can see from Eq. (6) that the exciting-photon energy dependence of the total fluorescence intensity is determined by the cross section for population of the initial fluorescence state. Therefore, experimental intensities $I^{Xv''}_{Av'}(\omega)$ are compared in the panels (a) of Figs. 5–8 with the theoretical cross sections $\sigma_{Av'}(\omega)$. The measured intensities are normalized to the computed cross sections at the position of the $v_r=0$ vibration level. From these figures good overall agreement between the measured fluorescence intensities and computed photoionization cross sections can bee seen. A small disagreement is possibly due to the photoelectron impact induced fluorescence and additional population of the final $A\ ^2\Pi(v')$ states via radiative cascade decay of highly excited ionic states.

The present polarization analysis of the resonantly excited $CO^+(A\ ^2\Pi \rightarrow X\ ^2\Sigma^+)$ fluorescence discloses a slight anisotropy in the fluorescence emission with a small negative angular distribution parameter, depicted in panels (c) of Figs. 5–8 by open circles. As seen from Eq. (21), parameter $\beta 2$ is proportional to the difference between intensities $I_{\perp} - I_{\parallel}$. In the present case ($|\beta 2| \ll 1$), this difference is by one order of magnitude smaller than the intensities themselves. The latter fact leads to large experimental uncertainties in the determination of the parameter $\beta 2$ (typical experimental errors are indicated by bars for selected energy points). The figures illustrate overall agreement between signs and absolute values of the measured and computed $\beta 2^{Xv''}_{Av'}(\omega)$ parameters around the $v_r=0-2$ resonances. The average curvatures of the measured and computed parameters have similar tendency. In the majority of the cases the measured dispersions $\beta 2^{Xv''}_{Av'}(\omega)$ possess also similar variations across the resonances v_r, supporting the impact of the nuclear vibrational motion illustrated by theory.

The absolute values of the measured $\beta 2^{Xv''}_{Av'}(\omega)$ parameters in Figs. 5–8 are systematically lower than the computed ones. A possible reason might be an additional population of the initial fluorescence state $A\ ^2\Pi(v')$ via radiative cascades of highly excited ionic states. The latter effect in atoms causes disalignment of the initial fluorescence state and leads to a decrease of the absolute value of $\beta 2$ (see, e.g., [3] and references therein). In addition, molecular rotational motion not included in the present calculations can be a reason for the decrease of the absolute value of $\beta 2$. The radiative decay lifetime of the $CO^+(A\ ^2\Pi)$ state, estimated from the fluorescence width [Eq. (8)], is about 2.5 μs. Rotational splittings of the individual $A\ ^2\Pi(v',J') \rightarrow X\ ^2\Sigma^+(v'',J'')$ fluorescence lines (not resolved in the present experiment) is by orders of magnitude larger than their radiative width [18]. Thus, during the radiative decay lifetime the total electronic angular momentum $L'+S'$ has enough time to precess around the total angular momentum $J'=L'+S'+R'$, where R' is the angular momentum due to nuclear rotation, resulting in a disalignment of the $CO^+(A\ ^2\Pi)$ ionic state [45]. An investigation of the above effects is outside the scope of the present paper.

V. SUMMARY

Dispersions of the angular distribution parameters for the $CO^+(A\ ^2\Pi)$ photoelectrons, $\beta^e_{Av'}(\omega)$, and for the $CO^+(A\ ^2\Pi \rightarrow X\ ^2\Sigma^+)$ fluorescence, $\beta 2^{Xv''}_{Av'}(\omega)$, have been calculated in the vicinity of the $1s^{-1}\pi^*$ resonance of the C^*O molecule. For this purpose basic equations describing the angular distribution of fluorescence radiation in diatomic molecules are derived. The potential energy curves of the relevant states and bound molecular orbitals of the CO molecule were computed within the MO LCAO approach, whereas the single center (SC) method with precise molecular field potentials was applied in order to compute partial waves for the photoelectron in the continuous spectrum. In the calculations, the interference between the different resonant and direct photoionization channels was taken into account. The computed absolute direct photoionization cross section, oscillator strength for the $1s^{-1}\pi^*$ excitation, and Auger decay rate are in good agreement with the experimental data from [8,44]. The computed relative intensities of the participator $1s^{-1}\pi^*(v_r) \rightarrow A\ ^2\Pi(v')$ RA spectra agree well with the experimental [13] ones.

The direct transition amplitude and the lifetime vibrational interference (LVI) effects cause significant changes of the computed angular distribution parameters with respect to the 2ST model. The interference between dominating resonant and weak direct transition amplitudes causes the long-range exciting-photon energy dependencies of the $\beta^e_{Av'}(\omega)$ and $\beta 2^{Xv''}_{Av'}(\omega)$. In the presence of the direct photoionization channel, LVI gives rise to significant variations of the computed parameters across the positions of the v_r vibrational levels of the intermediate resonance. The present theoretical results explain substantial variations of the Auger electron angular distribution parameters observed in [13] for the decay of the resonantly excited $C^*O(v_r)$ vibronic states into vibrationally resolved final Auger states.

In order to measure the angular distribution of the resonantly excited $CO^+(A\ ^2\Pi \rightarrow X\ ^2\Sigma^+)$ fluorescence, polarization analysis of the fluorescence intensities in the wavelength range between 378 and 578 nm has been performed by photon-induced fluorescence spectroscopy in the exciting-photon energy range between 287.08 and 288.02 eV within

the Raman regime for the C^*O excitation. The presently measured parameters $\beta 2_{Av'}^{Xv''}(\omega)$ are in good qualitative agreement with the theoretical ones. Nonconstant dependencies of the experimental $\beta 2_{Av'}^{Xv''}(\omega)$ on ω confirm that the nuclear dynamics influences the angular distribution of fluorescence radiation in molecules. However, the small absolute value of the angular distribution parameter of the $CO^+(A \rightarrow X)$ fluorescence makes it difficult to quantitatively confirm predicted dispersions experimentally. The $1s^{-1}\pi^*$ excitations of the NO and N_2 molecules can be suggested as the objects for angularly and vibrationally resolved resonant Auger and fluorescence spectroscopies.

ACKNOWLEDGMENTS

This work was performed within the European Community's 7th Framework Programme (Marie Curie Project No. PIIF-GA-2008-219224) and the Deutsche Forschungsgemeinschaft's (DFG) project (Project No. EH 187/16-1). The Helmholtz-Zentrum Berlin is gratefully acknowledged for travel expense support by Bundesministerium für Bildung und Forschung (BMBF) Contract No. 05 ES3XBA/5. V.L.S. and I.D.P. would like to thank the Institute of Physics, University of Kassel for the hospitality during their stay there.

[1] N. A. Cherepkov and S. K. Semenov, J. Phys. B **37**, 1267 (2004).
[2] E. G. Berezhko and N. M. Kabachnik, J. Phys. B **10**, 2467 (1977).
[3] B. M. Lagutin, I. D. Petrov, V. L. Sukhorukov, Ph. V. Demekhin, B. Zimmermann, S. Mickat, S. Kammer, K.-H. Schartner, A. Ehresmann, Y. A. Shutov, and H. Schmoranzer, J. Phys. B **36**, 3251 (2003).
[4] B. M. Lagutin, I. D. Petrov, V. L. Sukhorukov, S. Kammer, S. Mickat, R. Schill, K.-H. Schartner, A. Ehresmann, Y. A. Shutov, and H. Schmoranzer, Phys. Rev. Lett. **90**, 073001 (2003).
[5] K.-H. Schartner, R. H. Schill, D. Hasselkamp, S. Mickat, S. Kammer, L. Werner, S. Klumpp, A. Ehresmann, H. Schmoranzer, B. M. Lagutin, and V. L. Sukhorukov, J. Phys. B **38**, 4155 (2005).
[6] N. M. Kabachnik, S. Fritzsche, A. N. Grum-Grzhimailo, M. Meyer, and K. Ueda, Phys. Rep. **451**, 155 (2007).
[7] C. M. Truesdale, D. W. Lindle, P. H. Kobrin, U. E. Becker, H. G. Kerkhoff, P. A. Heimann, T. A. Ferrett, and D. A. Shirley, J. Chem. Phys. **80**, 2319 (1984).
[8] O. Hemmers, in *Studies of Vacuum Ultraviolet and X-Ray Processes*, edited by U. Becker (AMS Press, New York, 1993), Vol. 3.
[9] G. Prümper, D. Rolles, H. Fukuzawa, X. J. Liu, Z. Pešic, I. Dumitriu, R. R. Lucchese, K. Ueda, and N. Berrah, J. Phys. B **41**, 215101 (2008).
[10] V. Carravetta, F. K. Gel'mukhanov, H. Ågren, S. Sundin, S. J. Osborne, A. Naves de Brito, O. Björneholm, A. Ausmees, and S. Svensson, Phys. Rev. A **56**, 4665 (1997).
[11] M. N. Piancastelli, M. Neeb, A. Kivimäaki, B. Kempgensy, H. M. Köppe, K. Maier, A. M. Bradshaw, and R. F. Fink, J. Phys. B **30**, 5677 (1997).
[12] S. J. Osborne, S. Sundin, A. Ausmees, S. L. Sorensen, A. Kikas, and S. Svensson, J. Electron Spectrosc. Relat. Phenom. **95**, 25 (1998).
[13] E. Kukk, J. D. Bozek, W. Cheng, R. F. Finka, A. A. Wills, and N. Berrah, J. Chem. Phys. **111**, 9642 (1999).
[14] Z. W. Gortel, R. Teshima, and D. Menzel, Phys. Rev. A **58**, 1225 (1998).
[15] S. Bonhoff, K. Bonhoff, and K. Blum, J. Phys. B **32**, 1139 (1999).
[16] R. F. Fink, M. N. Piancastelli, A. N. Grum-Grzhimailo, and K. Ueda, J. Chem. Phys. **130**, 014306 (2009).
[17] F. K. Gel'Mukhanov, L. N. Mazalov, and A. V. Kondratenko, Chem. Phys. Lett. **46**, 133 (1977).
[18] P. H. Krupenie, Natl Std. Ref. Data Ser. Natl Bur. Std. (US) **5**, 1 (1966).
[19] A. Ehresmann, W. Kielich, L. Werner, Ph. V. Demekhin, D. V. Omel'yanenko, V. L. Sukhorukov, K.-H. Schartner, and H. Schmoranzer, Eur. Phys. J. D **45**, 235 (2007).
[20] A. Ehresmann, L. Werner, S. Klumpp, S. Lucht, H. Schmoranzer, S. Mickat, R. Schill, K.-H. Schartner, Ph. V. Demekhin, M. P. Lemeshko, and V. L. Sukhorukov, J. Phys. B **39**, 283 (2006).
[21] Ph. V. Demekhin, V. L. Sukhorukov, W. Kielich, L. Werner, S. Klumpp, A. Ehresmann, K.-H. Schartner, and H. Schmoranzer, J. Phys. B **41**, 045104 (2008).
[22] A. Ehresmann, L. Werner, S. Klumpp, H. Schmoranzer, Ph. V. Demekhin, B. M. Lagutin, V. L. Sukhorukov, S. Mickat, S. Kammer, B. Zimmermann, and K.-H. Schartner, J. Phys. B **37**, 4405 (2004).
[23] Ph. V. Demekhin, D. V. Omel'yanenko, B. M. Lagutin, V. L. Sukhorukov, L. Werner, A. Ehresmann, K.-H. Schartner, and H. Schmoranzer, Opt. Spectrosc. **102**, 318 (2007).
[24] A. Ehresmann, Ph. V. Demekhin, W. Kielich, I. Haar, M. A. Schlüter, V. L. Sukhorukov, and H. Schmoranzer, J. Phys. B **42**, 165103 (2009).
[25] G. Herzberg, *Molecular Spectra and Molecular Structure: I. Spectra of Diatomic Molecules*, 2nd ed. (Van Nostrand Reinhold Company, Cincinnati, Toronto, New York, Melbourne, London, 1950).
[26] N. A. Cherepkov, J. Phys. B **14**, 2165 (1981).
[27] J. C. Tully, R. S. Berry, and B. J. Dalton, Phys. Rev. **176**, 95 (1968).
[28] A. D. Buckingham, B. J. Orr, and J. M. Sichel, Philos. Trans. R. Soc. London, Ser. A **268**, 147 (1970).
[29] I. I. Sobelman, *Introduction to the Theory of Atomic Spectra*, 1st ed. (Pergamon Press, Oxford, New York, Toronto, 1972).
[30] H. Schmoranzer, S. Lauer, F. Vollweiler, A. Ehresmann, V. L. Sukhorukov, B. M. Lagutin, I. D. Petrov, Ph. V. Demekhin, K.-H. Schartner, B. Magel, and G. Mentzel, J. Phys. B **30**, 4463 (1997).
[31] http://classic.chem.msu.su/gran/gamess/index.html
[32] M. W. Schmidt *et al.*, J. Comput. Chem. **14**, 1347 (1993).

[33] T. H. Dunning, Jr., J. Chem. Phys. **55**, 716 (1971).
[34] K. P. Huber and G. Herzberg, *Molecular Spectra and Molecular Structure. IV. Constants of Diatomic Molecules* (Van Nostrand Reinhold Company, New York, 1979).
[35] K. C. Prince, M. Vondráček, J. Karvonen, M. Coreno, R. Camilloni, L. Avaldi, and M. de Simone, J. Electron Spectrosc. Relat. Phenom. **101-103**, 141 (1999).
[36] D. M. Bishop, Adv. Quantum Chem. **3**, 25 (1967).
[37] V. L. Sukhorukov, V. F. Demekhin, V. A. Yavna, I. D. Petrov, L. A. Demekhina, and S. V. Lavrentiev, Coord. Chem. (Sov.) **9**, 158 (1983).
[38] P. G. Burke and M. J. Seaton, *Atomic and Molecular Scattering*, Methods in Computational Physics Vol. 10, (Academic Press, London, 1971), Chap.: Numerical Solutions of the Integro-Differential Equations of Electron-Atom Collision Theory, pp. 1–80.
[39] A. F. Starace, *Theory of Atomic Photoionization*, Handbuch der Physik Vol. 31 (Springer, Berlin, 1982).
[40] K. Smith, R. J. W. Henry, and P. G. Burke, Phys. Rev. **147**, 21 (1966).
[41] T. Åberg and B. Crasemann, *Resonant Anomalous X-ray Scattering: Theory and Experiment* (North-Holland, Amsterdam, 1994).
[42] T. Åberg, Phys. Rev. **156**, 35 (1967).
[43] A. P. Jucys and A. J. Savukinas, *Mathematical Foundation of the Atomic Theory*, 1st ed. (Mintis, Vilnius, 1973) (in Russian).
[44] R. B. Kay, P. E. Van der Leeuw, and M. J. Van der Wiel, J. Phys. B **10**, 2513 (1977).
[45] K. Blum, *Density Matrix Theory and Applications*, 2nd ed. (Plenum, New York, 1996).
[46] H. Schmoranzer, H. Liebel, F. Vollweiler, R. Müller-Albrecht, A. Ehresmann, K.-H. Schartner, and B. Zimmermann, Nucl. Instrum. Methods Phys. Res. A **467-468**, 1526 (2001).
[47] B. Zimmermann, O. Wilhelmi, K.-H. Schartner, F. Vollweiler, H. Liebel, A. Ehresmann, S. Lauer, H. Schmoranzer, B. M. Lagutin, I. D. Petrov, and V. L. Sukhorukov, J. Phys. B **33**, 2467 (2000).
[48] *NIST Atomic Spectra Database* (National Institute of Standards and Technology, Gaithersburg, MD, 2008), http://physics.nist.gov/PhysRefData/ASD/index.html